Li *et al. Energy Mater.* **2025**, *5*, 500096
DOI: 10.20517/energymater.2024.312

Energy Materials

Article

Open Access

Check for updates

High-valence molybdenum-induced boundary-rich heterostructures for enhanced oxygen evolution reaction

Lu Li[1,#], Jinhu Wu[1,#], Limeng Sun[1], Fengying Pan[1], Dongfang Li[2], Xianjun Cao[1,*], Li Gao[1], Yuxia Zhang[3], Hong Gao[1], Qing Li[4], Jinqiang Zhang[2,*], Yufei Zhao[2,*], Hao Liu[2,*]

[1]Joint International Laboratory on Environmental and Energy Frontier Materials, School of Environmental and Chemical Engineering, Shanghai University, Shanghai 200444, China.
[2]Centre for Clean Energy Technology, University of Technology Sydney, Broadway, Sydney, NSW 2007, Australia.
[3]School of Materials Science and Engineering, Shijiazhuang Tiedao University, Shijiazhuang 050043, Hebei, China.
[4]State Key Laboratory of Material Processing and Die & Mould Technology, School of Materials Science and Engineering, Huazhong University of Science and Technology, Wuhan 430074, Hubei, China.

[*]**Correspondence to:** Dr. Xianjun Cao, Joint International Laboratory on Environmental and Energy Frontier Materials, School of Environmental and Chemical Engineering, Shanghai University, No. 99, Shangda Road, Baoshan District, Shanghai 200444, China. E-mail: ascaoxj@shu.edu.cn; Dr. Yufei. Zhao, Dr. Jinqiang Zhang and Prof. Hao Liu, University of Technology Sydney, PO Box 123, Ultimo NSW 2007, Australia. E-mail: Yufei.zhao@uts.edu.au; Jinqiang.zhang@uts.edu.au; Hao.liu@uts.edu.au

How to cite this article: Li, L.; Wu, J.; Sun, L.; Pan, F.; Li, D.; Cao, X.; Gao, L.; Zhang, Y.; Gao, H.; Li, Q.; Zhang, J.; Zhao, Y.; Liu, H. High-valence molybdenum-induced boundary-rich heterostructures for enhanced oxygen evolution reaction. *Energy Mater.* **2025**, *5*, 500096. https://dx.doi.org/10.20517/energymater.2024.312

Received: 31 Dec 2024 **First Decision:** 22 Jan 2025 **Revised:** 23 Feb 2025 **Accepted:** 27 Feb 2025 **Published:** 30 Apr 2025

Academic Editor: Yuhui Chen **Copy Editor:** Ping Zhang **Production Editor:** Ping Zhang

Abstract

The green synthesis of hydrogen through electrochemical water splitting has been severely limited by the slow kinetics of the anodic oxygen evolution reaction (OER). However, the current benchmark electrocatalysts are still based on precious metals. Therefore, developing low-cost and highly efficient OER electrocatalysts is of great importance. Here, we design nanoscale multicomponent metal flakes with a crystalline/amorphous structure (ac-FeCoNiMo) via a simple sol-gel strategy to enhance OER performance. By engineering the structure through a high-valence Mo doping strategy, we successfully develop ac-FeCoNiMo with a unique architecture featuring boundary-rich regions, modulated Fe/Co species, defects, and enlarged metal-O bonds. As a result, the optimized ac-FeCoNiMo exhibits excellent electrochemical OER performance, achieving low overpotentials of 222 mV and 253 mV to reach current densities of 20 mA cm^{-2} and 100 mA cm^{-2}, respectively, along with outstanding stability. Mechanistic investigations reveal that ac-FeCoNiMo follows the Lattice Oxygen Mediated mechanism during the OER process. This behavior is likely due to the induced weakening of metal-oxygen bonds, resulting from the

expanded M-O-M (M = metal) units and the formation of abundant boundary-rich regions. This study paves the way for the development of highly efficient multi-element electrocatalysts.

Keywords: High-valence molybdenum, modulated Fe/Co species, enlarged metal-O bonds, oxygen evolution reaction

INTRODUCTION

Green hydrogen has been extensively studied as a renewable energy to replace fossil fuels[1-4]. Electrochemical water splitting is one of the most efficient strategies to enable the production of hydrogen with zero CO_2 emission[5-7]. However, the slow kinetics of the oxygen evolution reaction (OER) at the anode side of water splitting severely hinders its further commercialization[8,9]. Currently, precious metal electrocatalysts based on ruthenium (Ru) and iridium (Ir) are still the most widely used and active OER electrocatalysts[10]. Nevertheless, their low abundance and high cost highly impede their further application. Alternatively, transition metal-based catalysts, e.g., iron/cobalt/nickel (Fe/Co/Ni), have exhibited promising OER activity and stability in alkaline conditions, with the advantage of abundant distribution and low-cost properties[11,12]. The intrinsic structures of transition metal compounds are suitable for OER, but their catalytic activity is still far from satisfactory[12,13]. Therefore, developing novel strategies to engineer Fe/Co/Ni-based materials to achieve boosted OER performance is desired.

One strategy is to incorporate foreign elements to boost the OER catalytic performance by modulating the electronic structure of Fe/Ni/Co species and facilitating electron transportation[14,15]. Especially, the doped high valence state elements can induce strong electronic interaction between high valence state metal atoms and Fe/Co/Ni species, which can significantly modulate the corresponding properties to further effectively promote the pre-activation process of Fe/Co/Ni-based catalysts to optimize their OER performance. Recently, the high valence element Mo has been investigated as the doping agent to engineer Fe, Co or Ni-based OER electrocatalysts for enhanced performance[16]. For instance, Mo-doped $Co(OH)_2$ nanofilms coupled with CoP nanosheets [$MoCo(OH)_2$/CoP/NF] supported on the nickel foam have been designed for oxygen generation[17]. The incorporation of element Mo reduced the thickness of the $Co(OH)_2$ nanosheets and induced the formation of porous folded structure, leading to the increased active sites. In addition, Mo and Fe co-doped $Ni(OH)_2$/NiOOH nanosheets showed a significant synergistic effect between Mo, Fe and Ni atoms, which increased the interaction between *OH and the active sites, and thus improved the OER activity[18]. MoFe:$Ni(OH)_2$/NiOOH only required the overpotential of 280 mV at the current density of 100 mA cm^{-2}, and no sign of degradation was observed after 50 h testing. Furthermore, Mo-doped nickel cobaltate OER electrocatalyst resulted in the formation of the porous and layered structure, which effectively increased the specific surface area and electron transfer, leading to enhanced OER activity[19].

Besides doping strategy, amorphization and defects in metal-based materials can also influence the electronic structure to engineer the active sites, and thus improve the OER performance[20,21]. However, excessive defect sites may result in poor conductivity and decrease the OER performance. Thus, alloying amorphous oxides with crystalline oxides forming crystalline/amorphous heterostructures may have excellent OER electrocatalytic activity due to their combined advantages[22]. For example, the crystalline FeOOH combined with amorphous FeOOH phase boundaries (a-c-FeOOH) has shown superior OER activity compared to that of amorphous FeOOH or crystalline FeOOH (a-c-FeOOH:300 mA cm^{-2}@330 mV, a-FeOOH:47 mA cm^{-2}@330 mV, c-FeOOH: 60 mA cm^{-2}@330 mV)[23]. Moreover, Fe-doped Ni-Co photosensitive electrocatalyst (Fe-NiCoHPi) with the amorphous shell and crystal core has increased the active sites and conductivity, respectively[24]. As a result, Fe-NiCoHPi delivered current densities of

15 mA cm^{-2} and 100 mA cm^{-2} at 206 mV and 257 mV overpotentials. Similarly, the crystalline Ag and amorphous NiCoMo oxides with a dense crystalline/amorphous interface can adjust the electronic structure of the interface sites, optimize the adsorption energy of reaction intermediates, and stabilize the transformed active phase, thus significantly accelerating the OER kinetics and stability[25].

Herein, we successfully applied sol-gel and annealing strategies to prepare the nanoscale polymetallic crystalline/amorphous coexisting FeCoNiMo flasks with abundant boundary structures (ac-FeCoNiMo) induced by high valence state of the Mo element. It also engineers the electronic structure of Fe/Co and achieves decreased valence states due to the electron transfer between Fe/Co and Mo. Therefore, the resulting ac-FeCoNiMo has exhibited superior OER electrocatalytic activity compared to benchmark RuO_2, with a low overpotential of 208 mV at the current density of 10 mA cm^{-2}, and a Tafel slope of 38.86 mV dec^{-1}. Moreover, the OER activity of FeCoNiMo shows no visible decay before and after 10,000 cycles, demonstrating excellent long-term stability. Furthermore, the enlarged metal-O bond length results in weakened bond strength, thus favoring the Lattice Oxygen Mediated (LOM) mechanism for ac-FeCoNiMo, boosting its corresponding OER catalytic capability. This work reveals the activity mechanism of its lattice oxygen (O_L), thus providing a method for the design of highly active and durable OER electrocatalysts.

EXPERIMENTAL

Materials

Chemicals including ethanol (C_2H_6O, A.R.) and acetone (C_3H_6O, A.R.) were purchased from China National Pharmaceutical Group Chemical Reagent Co., Ltd and used as received. Chemicals including iron chloride ($FeCl_3$, A.R.), nickel chloride ($NiCl_2$, A.R.), cobalt chloride ($CoCl_2$, A.R.) and Nafion®117 (5 wt.%) were purchased from Sigma-Aldrich and used as received. Molybdenum ($MoCl_5$, A.R.) and epoxy propane (C_3H_6O, A.R.) were purchased from Shanghai Titan Chemical Co., Ltd and used as received.

Synthesis of ac-FeCoNiMo

As shown in Supplementary Figure 1, ac-FeCoNiMo was prepared according to the reported methods[1,2]. Briefly, 0.2 mL of deionized water, 2 mL of ethanol and 1 mL of epoxy propane were added to a solution mixed with 0.07 mmol of anhydrous iron chloride, 0.07 mmol of anhydrous cobalt chloride, 0.07 mmol of anhydrous nickel chloride, and 0.07 mmol of anhydrous molybdenum chloride and 4 mL of anhydrous ethanol. The mixed solution was then stirred overnight and aged in acetone for one week to obtain the ac-FeCoNiMo sol-gel. The ac-FeCoNiMo sol-gel was dried at 50 °C and then heated at 400 °C for 2 h to obtain ac-FeCoNiMo.

Synthesis of the comparison materials

The synthesis procedures of the controls were the same as those of ac-FeCoNiMo, without the addition of anhydrous molybdenum chloride for FeCoNi, anhydrous nickel chloride for FeCoMo, and anhydrous cobalt chloride for FeNiMo, respectively.

Characterization

The material morphology details and structural information were obtained using a Transmission Electron Microscope (TEM, JEOL 2100F) and X-ray Diffraction (XRD, 3 KW D/MAX2200V, step size of 0.02°, scanning rate of 8° min^{-1}), and the sample elemental content and distribution were studied by Energy Dispersive X-ray spectroscopy (EDX) combined with TEM and Aglient 7800 Inductively coupled plasma-Mass Spectrometry (ICP-MS). In addition, the information related to the specific surface area and pore structure of the material was obtained via conducting Brunauer-Emmett-Teller (BET) analysis on the sample and combining it with the Barrett-Joyner-Halenda (BJH) method.

Electrocatalytic measurements

For electrode preparation, 500 μL of ethanol, 10 μL of Nafion and 2 mg of catalyst were used to prepare electrode slurry, then dripped onto carbon paper to obtain the working electrode with the catalyst load of 2 mg cm^{-2}. The Pt wire and Hg/HgO/OH (1 M KOH) electrode were used as the counter electrode and reference electrode, respectively. Subsequently, a series of electrochemical tests including cyclic voltammetry (CV), linear sweep voltammetry (LSV), and electrochemical impedance spectroscopy (EIS) were conducted in the standard three-electrode system using the CHI 760E electrochemical workstation. The EIS test was conducted at a voltage of 1.45 V versus reversible hydrogen electrode (RHE), with the frequency range of the amplitude from 0.1 Hz to 10^6 Hz.

Using the Nernst equation to convert the $E_{Hg/HgO/OH}$ to E_{RHE}:

$$E_{RHE} = E_{Hg/HgO} + 0.098 + 0.059 * \text{pH} \quad (1)$$

LSV test was measured in 1 M KOH at the scan rate of 10 mV s^{-1} over the range of 0.2 V to 0.9 V versus RHE. Here, the CV test was used for the stability test with the range of 0.2 V to 0.6 V versus RHE at the sweep rate of 100 mV s^{-1} for 10,000 cycles. Through the LSV before and after the CV, its stability was evaluated.

The turnover frequency (TOF) is a key metric to evaluate the intrinsic catalytic activity of an OER catalyst, which can be calculated using

$$TOF = \frac{I}{4nF} \quad (2)$$

where the factor 4 accounts for the four-electron process involved in O_2 evolution from water, I is the current (A) at corresponding overpotential from LSV curves, F is Faraday constant (96,485 C mol^{-1}), and n is number of active sites. We assume that all metal sites are active sites for OER, and we can derive

$$TOF_{surface} = \frac{I N_A}{4NmFS_g} \quad (3)$$

Where S_g is the specific surface area value. N represents the number of surface atoms, m is the mass of the load per square centimeter, and N_A represents Avogadro's constant.

The long stability test was conducted in a three-electrode system using a constant-current mode. The working electrode, counter electrode, and reference electrode were the same as those in the LSV polarization curve experiment.

RESULTS AND DISCUSSION

Structural analysis of materials

The ac-FeCoNiMo was prepared by a sol-gel method which relies on controlling the hydrolysis of metal chlorides in the mixture of water and ethanol [Supplementary Figure 1]. Epoxy propane was added as a complexing agent and a gel initiator to coordinate with metal ion hydrates while promoting gelation via subsequent metal salt hydrolysis and polycondensation[26]. As a result, the color of the mixture gradually turned from clear to black, and eventually brownish green. Followed by a subsequent calcination treatment, the nanoscale multicomponent metal flakes with crystalline/amorphous structure (ac-FeCoNiMo) were achieved. The ICP-MS analysis confirmed the elemental compositions of Fe, Co, Ni, and Mo are 16.16 wt.%, 16.41 wt.%, 14.61 wt.%, and 27.72 wt.%. FeCoNi with no Mo incorporation has also been prepared using the

same method as a comparison.

The XRD was further performed on ac-FeCoNiMo and FeCoNi to investigate the crystal structure. The results in Figure 1A show the peaks of 31.1°, 36.7°, 44.6°, 59.1°, and 64.9° in FeCoNi correspond to the crystal planes of FeCoNi oxide. However, no sharp characteristic peaks are observed for FeCoNiMo, suggesting much lower crystallinity. Therefore, the introduction of high valence Mo element can efficiently cause the decreased crystallinity of FeCoNi, which may contribute to the catalytic activity.

The as-synthesized ac-FeCoNiMo is further characterized by TEM. The TEM images in Figure 1B and C and Supplementary Figure 2 confirm that the achieved FeCoNiMo nanosheets contain both crystalline and amorphous structures (red box), which is consistent with the XRD result (lower crystallinity)[27]. The formed crystalline and amorphous structures result in the formation of abundant atomic boundaries and the atoms located at the boundary sites may display distorted coordinating states, to boost the OER activity[28,29]. In contrast, FeCoNi with no Mo incorporation shows a similar nanosheet nanostructure to that of ac-FeCoNiMo, but it exhibits much higher crystallinity properties (no amorphous structures have been observed) [Supplementary Figure 3]. The above results indicate that Mo interacts with other elements (Fe, Co, Ni) during the formation of the crystal structure, hindering the orderly growth of the crystals. In addition, the high-resolution transmission electron microscopy (HRTEM) images [Supplementary Figure 4] of ac-FeCoNiMo show that the spacing of the lattice fringe was 0.2 nm, 0.24 nm, and 0.275 nm, which are larger than those of FeCoNi with the spacing of lattice fringes of 0.148 nm and 0.203 nm [Supplementary Figure 5], indicating the introduction of Mo doping with higher atomic radius can effectively lead to the lattice deformation and enlarge the lattice spacing[30]. The element mapping results of ac-FeCoNiMo in Figure 1d-g reveal the homogeneous distribution of Fe, Ni, Co, and Mo in the structure, confirming the successful preparation of multicomponent metal oxides.

BET analysis was conducted on ac-FeCoNiMo and FeCoNi to characterize their specific surface area and pore size distribution. The nitrogen adsorption and desorption curve of ac-FeCoNiMo in Figure 2A is the typical Type II isotherm curve, which is different from the Type IV isotherm curve of FeCoNi. In addition, ac-FeCoNiMo exhibits much higher surface area and much smaller pore size distribution than FeCoNi [Supplementary Table 1]. This indicates that the introduction of Mo doping affected the micromorphology of ac-FeCoNiMo, leading to the increased specific surface area and optimized pore structure, to facilitate OER process[31-33]. The high surface area provides more catalytic sites for the OER, leading to a greater number of reaction sites available for water oxidation. Moreover, it allows better diffusion of reactants to the active sites and boosts the efficient removal of generated O_2 bubbles[34,35].

The survey X-ray Photoelectron Spectroscopy (XPS) spectrum of ac-FeCoNiMo verifies the presence of Fe, Ni, Co, Mo, and O elements, which is consistent with the results of ICP-MS and Energy Dispersive X-ray Spectroscopy (EDS) [Figure 2, Supplementary Tables 2 and 3]. The high-resolution Co 2p spectra of both ac-FeCoNiMo and FeCoNi [Figure 2B] show two pairs of peaks corresponding to Co^{2+} and Co^{3+}. These peaks shift negatively compared to those of FeCoNi (781.13 eV, 783.05 eV)[36]. Moreover, the ratio of Co^{3+} to Co^{2+} in FeCoNi and ac-FeCoNiMo obviously decreased from 1.37 to 0.59. Similarly, a decreased trend in the Fe^{2+}/Fe^{3+} is observed in ac-FeCoNiMo (1.71 to 1.23) [Figure 2C][37,38]. Therefore, the incorporation of high-valent Mo induces electron transfer between Co/Fe and Mo, resulting in a reduction in the valence states of Fe/Co species. This change in valence states affects the electronic structure of the material, which is of great significance for the OER catalytic activity. The high-resolution Ni 2p spectra of ac-FeCoNiMo and FeCoNi show similar peak positions and valence states [Figure 2D][39]. The high-resolution Mo 3d XPS spectrum [Figure 2E] shows a pair of peaks at 232.2 eV and 235.27 eV, corresponding to the $3d^{5/2}$ and $3d^{3/2}$

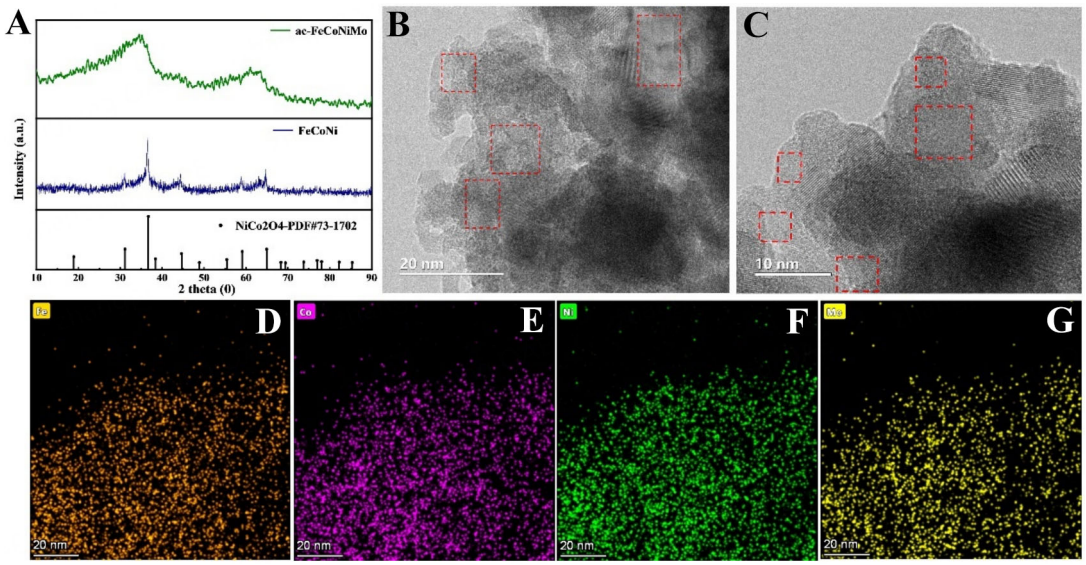

Figure 1. (A) XRD spectra of ac-FeCoNiMo and FeCoNi (B and C) TEM images of ac-FeCoNiMo, with the red dashed frame showing the amorphous structure region; (D-G) elemental mappings of ac-FeCoNiMo. XRD: X-ray diffraction; TEM: transmission electron microscope.

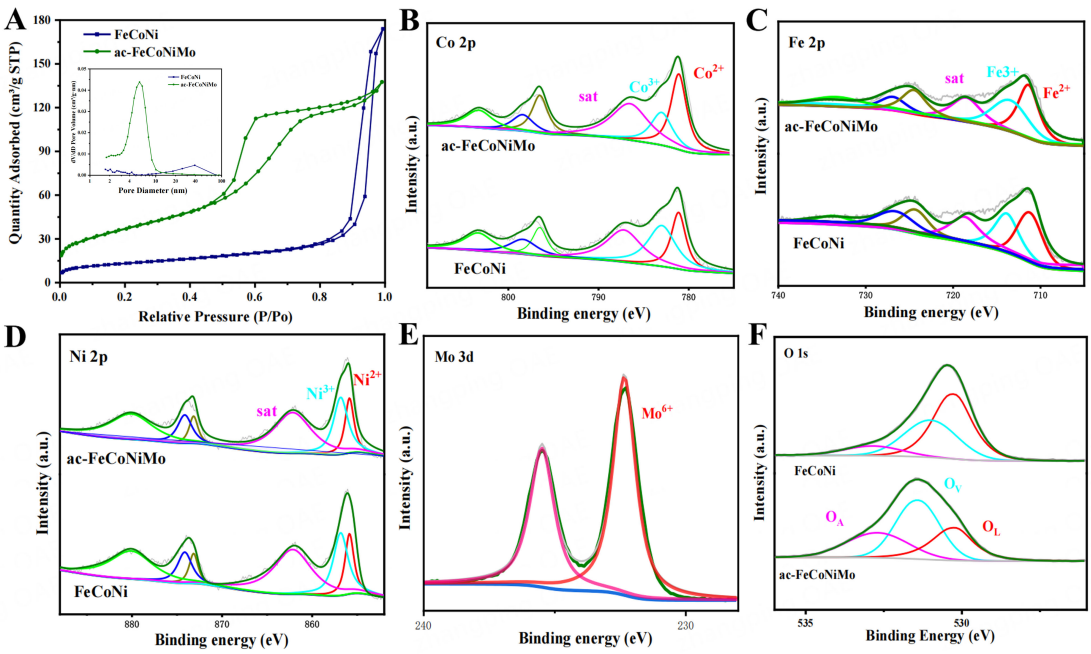

Figure 2. (A) Nitrogen desorption curve and pore distribution diagram of ac-FeCoNiMo and FeCoNi; (B-F) The high-resolution of Co 2p XPS spectra, Fe 2p XPS spectra, Ni 2p XPS spectra, Mo 3d XPS spectra and O 1s XPS spectra of ac-FeCoNiMo and FeCoNi. XPS: X-ray photoelectron spectroscopy.

of Mo^{6+}, respectively, indicating the presence of high valence Mo in ac-FeCoNiMo. The above results indicate the incorporation of high valence Mo induce the electron transfer between the Co/Fe and Mo elements, resulting in the formation of lower valence state of Fe/Co species, which may contribute to the

OER catalytic activity. In addition, the O 1s spectra of ac-FeCoNiMo [Figure 2F] correspond to O_L, oxygen vacancies (O_V), and surface adsorbed oxygen species (O_A) at 530.25 eV, 531.1 eV, and 532.84 eV, respectively[40-42]. Due to the crystalline/amorphous structure in ac-FeCoNiMo induced by high-valence Mo, the O_V content increased significantly compared to FeCoNi (from 38.6% to 44.8%), indicating that abundant defects have been created due to the incorporation of the Mo element. Compared with FeCoNi, the higher O_V ratio in ac-FeCoNiMo can accelerate electron transfer, expose more unsaturated metal sites as OER active sites, and modulate the electronic structure and intermediate adsorption energy.

For comparison, FeNiMo and FeCoMo were also prepared to investigate the multi-elements induced synergistic effect. The XRD results in Supplementary Figure 6 show that both FeNiMo and FeCoMo possess the same broadened and weakened XRD peak shape, indicating the presence of Mo may play an important role in the formation of low crystallinity structure.

To further elucidate the electronic structure, chemical state, and coordination environment of the synthesized ac-FeCoNiMo at the atomic level, X-ray absorption near-edge structure (XANES) and extended X-ray absorption fine structure (EXAFS) analyses were conducted on ac-FeCoNiMo. As depicted in Figure 3A, the K-edge absorption energies of the Fe for both ac-FeCoNiMo and FeCoNi are situated between the Fe foil and metal oxide, indicating that the valence state of Fe lies between 0 and +3. Moreover, the ac-FeCoNiMo shows a left position compared to FeCoNi, indicating a lower valence state of Fe species in ac-FeCoNiMo, which is consistent with the XPS results. Similarly, the lower valence state of Co species has also been observed for ac-FeCoNiMo [Figure 3B]. The XANES results further confirm the incorporation of high valence Mo induce the decreased valence state of Fe and Co species in ac-FeCoNiMo, suggesting electron transfer from the Mo element to the transition metals Fe and Co. The Fourier transforms of the EXAFS spectra (R space) of both Fe and Co species in Figure 3C and D show the dominant peak between 1-2 Å corresponding to the M-O (Fe/Co-O) coordination shell. Moreover, these peaks for Fe and Co all show obvious right peak shifts compared to the standard metal oxides (Fe_2O_3 and Co_3O_4), indicating the elongation of the M-O (Fe/Co) coordination bonds. The ac-FeCoNiMo with the incorporation of high valence Mo exhibits even enlarged bonds, which may be attributed to the formation of boundary-rich crystalline/amorphous heterostructures and Fe/Co-O-Mo. The enlarged bond lengths may result in the weakened metal-oxygen bond and activate the O_L to facilitate the OER process[43].

Electrocatalytic performance

The electrochemical performance was conducted using a three-electrode device in 1 M KOH solution at room temperature. As shown in Figure 4A and Supplementary Figure 7, ac-FeCoNiMo exhibits much lower overpotentials among all the samples with overpotentials of 222 mV and 253 mV to achieve the current densities of 20 mA cm^{-2} and 100 mA cm^{-2}, respectively, whereas 256 mV and 290 mV for FeCoNi, 274 mV and 332 mV for FeNiMo, 239 mV and 283 mV for FeCoMo, and 252 mV for RuO_2 at current densities of 20 mA cm^{-2}. Furthermore, Tafel curve analysis was performed based on LSV to evaluate its OER kinetics[44]. Figure 4B and Supplementary Figure 8 show the lowest Tafel slope for ac-FeCoNiMo, exhibiting faster OER kinetics and excellent OER intrinsic activity (ac-FeCoNiMo: 38.86 mV dec^{-1}, FeCoNi: 41.63 mV dec^{-1}, FeNiMo: 61.34 mV dec^{-1}, FeCoMo: 44.79 mV dec^{-1}, RuO_2: 81.71 mV dec^{-1}). It is worth mentioning that ac-FeCoNiMo also outperforms most non-noble metal OER electrocatalysts, with superior overpotential and Tafel slope at the current density of 10 mA cm^{-2} compared to most recent reports [Figure 4C and Supplementary Table 4]. The excellent OER performance of ac-FeCoNiMo should be attributed to the abundant active sites in boundary-rich crystalline/amorphous heterostructures, decreased valence state of Fe/Co species and also the formation of weakened Fe/Co-O-Mo bonds. EIS was performed to intuitively reflect the changes in charge transfer resistance (R_{ct}) of immobilized electrocatalysts during OER[45]. As shown in Figure 4D and Supplementary Figure 9, ac-FeCoNiMo exhibits the smallest semicircle of the

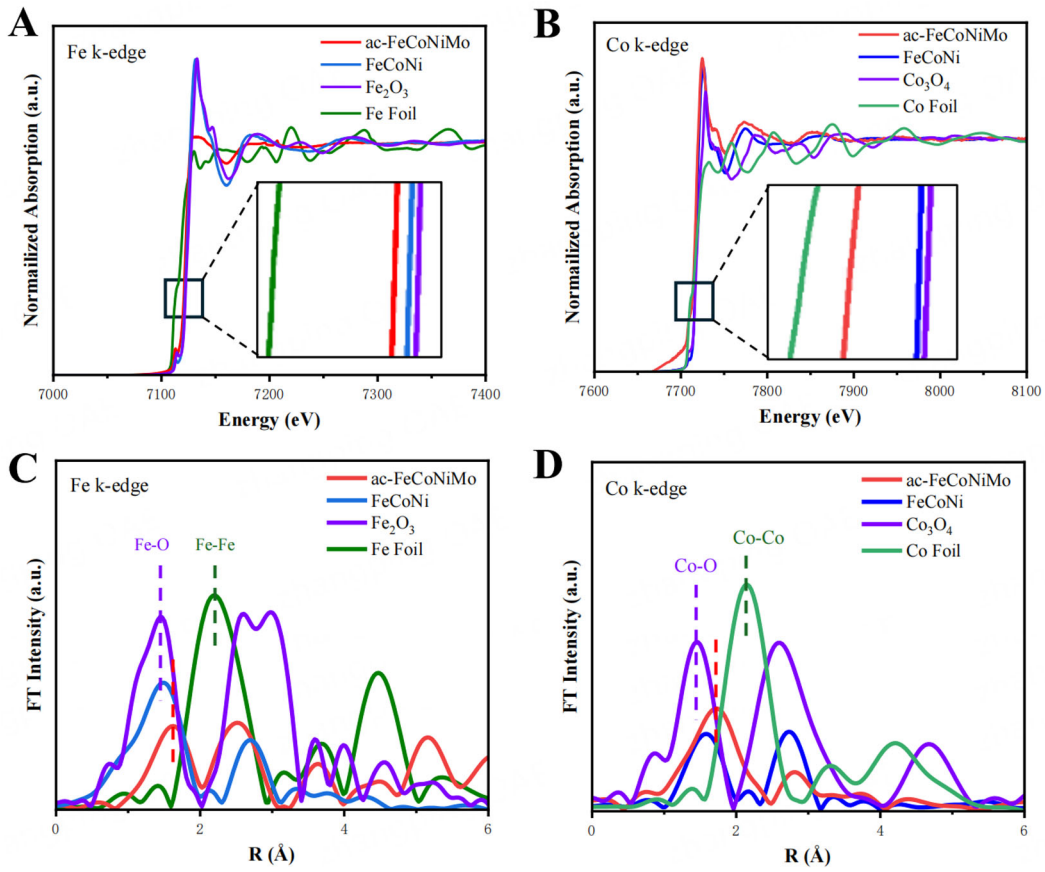

Figure 3. (A-D) XANES and EXAFS images of the ac-FeCoNiMo for Fe K-edge and Co K-edge. XANES: X-ray absorption near-edge structure; EXAFS: extended X-ray absorption fine structure.

lowest R_{ct}, indicating the fastest OER charge transfer rate compared to other candidates, consistent with Tafel analysis in Figure 4B. Therefore, the synergistic effect of boundaries, high surface area, high mass transfer efficiency [Supplementary Figure 10], modulated electronic structure and defects, in ac-FeCoNiMo guarantees abundant active sites and enhanced electronic conductivity, which ensures the highest OER activity.

TOF has been calculated to assess the intrinsic OER catalytic activity. As shown in Figure 4E, ac-FeCoNiMo exhibits the TOF of 0.0225 s^{-1} and 0.0375 s^{-1} at potentials of 1.47 V and 1.48 V, respectively, which is much higher than that of FeCoNi (0.012 s^{-1} and 0.0205 s^{-1}), demonstrating the superior intrinsic OER catalytic activity of ac-FeCoNiMo[46,47].

We further performed long-term stability tests on ac-FeCoNiMo by continuously running LSV tests. A comparison of LSV curves of ac-FeCoNiMo before and after 10000 CV cycles at the current density of 20 mA cm^{-2} in Figure 4F indicates negligible overpotential decay after long-term cycling. This verifies that ac-FeCoNiMo exhibits excellent long-term electrochemical stability for OER. Phased current testing was also conducted in addition to the long-term stability test. As shown in Figure 4G, we performed a constant-current test for 100 h. After operation at a current density of 100 mA cm^{-2}, the attenuation was negligible. This reflects that ac-FeCoNiMo exhibits significant reliability and practicality in the OER. These results evidently prove that ac-FeCoNiMo can tolerate high current density and maintain excellent

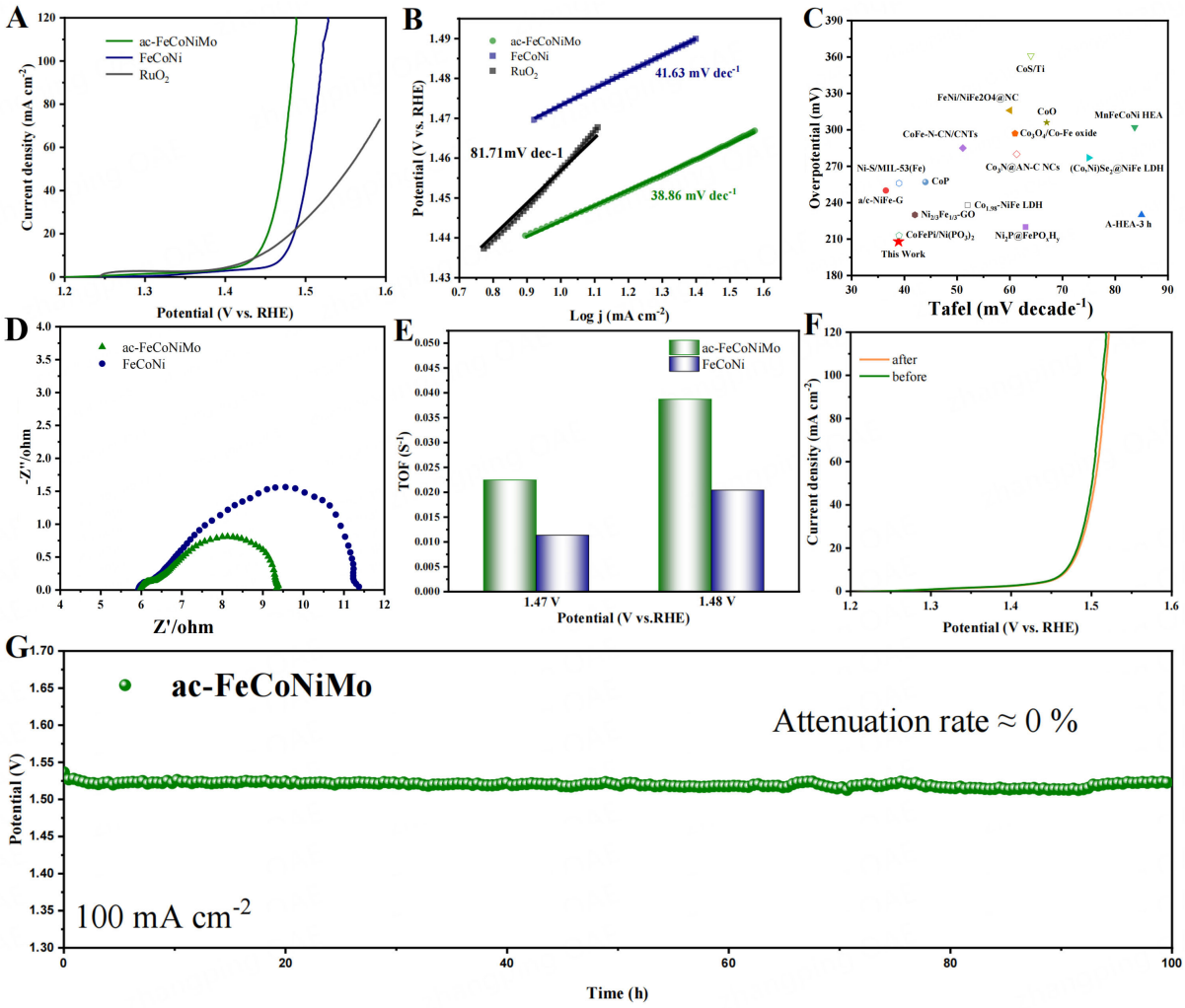

Figure 4. LSV curves (A) and Tafel curves (B) for ac-FeCoNiMo, FeCoNi, and RuO_2; (C) EIS diagram of ac-FeCoNiMo and FeCoNi (D) Coordinate diagram of OER electrocatalyst overpotential and Tafel slope; (E) The calculated TOF of ac-FeCoNiMo and FeCoNi at certain overpotentials; (F) LSV diagram of ac-FeCoNiMo before and after 10000 CV cycles of ac-FeCoNiMo and FeCoNi; (G) the long-term stability test of ac-FeCoNiMo. LSV: Linear sweep voltammetry; EIS: electrochemical impedance spectroscopy; OER: oxygen evolution reaction; TOF: turnover frequency.

stability[44]. After the stability tests, we conducted XRD and TEM characterizations of the ac-FeCoNiMo in Supplementary Figure 11. As can be observed from the XRD pattern, apart from the carbon peaks at around 26°, and 42.8°, there are no other diffraction peaks. Therefore, ac-FeCoNiMo after the reaction still exists in an amorphous form. The HRTEM images after the stability show that the boundary-rich crystalline-amorphous structure of ac-FeCoNiMo is well preserved.

The study of OER catalytic mechanism

The LOM involves non-coordinated proton-electron transfer steps at metal cation active sites and O_L. This mechanism is characterized by the presence of specific reaction intermediates Figure 5A, which serve as a basis for our assessment of the catalytic mechanism[48,49]. The superior catalytic activity of ac-FeCoNiMo over FeCoNi suggests the formed boundaries, decreased Fe/Co species and weakened Fe/Co-O bonds play a vital role in the OER process, which may change the catalytic mechanism. We have done the electrochemical performance test with and without TMA^+. A noticeable attenuation in the polarization

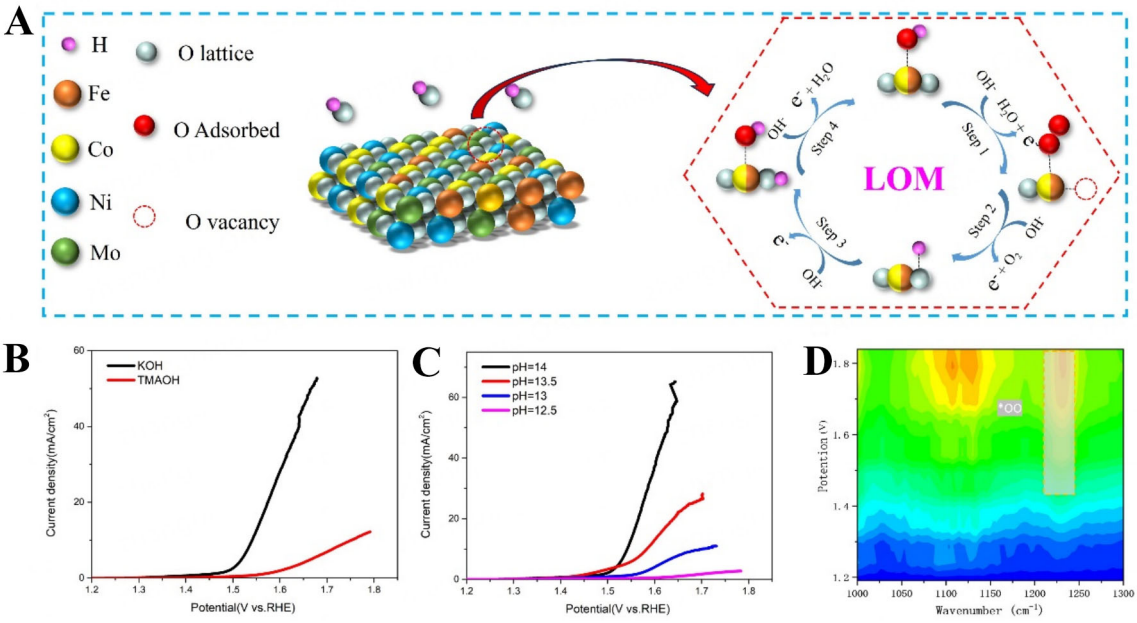

Figure 5. (A) LOM Mechanism (B)TMAOH Poisoning Experiment and (C) pH-Dependence Experiment of ac-FeCoNiMo; (D) *In situ* ATR-SEIRAS spectra at various applied potentials for ac-FeCoNiMo. LOM: Lattice oxygen mediated; ATR-SEIRAS: attenuated total reflection surface-enhanced infrared absorption spectroscopy; TMAOH: tetramethylammonium hydroxide.

curves is observed, suggesting the generation of $*O_2^{2-}$ intermediates during the catalytic process on ac-FeCoNiMo [Figure 5B]. As reported, the TMA^+ carries one unit of positive charge and has a large and regular tetrahedral spatial structure. Based on the principle of electrostatic interaction and spatial compatibility, the TMA^+ group can bind to negatively charged oxygen intermediates such as O_2^{2-} and O_2^-. Negatively charged oxygen intermediates are specific active intermediates in the LOM mechanism and do not appear in the adsorbate evolution mechanism (AEM). Therefore, the incorporation of TMA^+ strongly inhibits LOM mechanism in the OER reaction process, whereas it has little influence on the AEM, demonstrating that the OER process of ac-FeCoNiMo follows the LOM mechanism. We have also conducted LSV tests at varying pH values. A significant declined OER activity of ac-FeCoNiMo was observed when the pH decreased from 14.0 to 12.5 [Figure 5C], indicating a pH-dependent OER catalytic activity (AEM is primarily based on processes such as the adsorption and conversion of reactants at the active sites on the catalyst surface, and it does not change significantly with pH variations.), also indicating the OER catalytic mechanism of ac-FeCoNiMo follow the LOM process. To further investigate the catalytic mechanism, we have employed *in situ* attenuated total reflection surface-enhanced infrared absorption spectroscopy (ATR-SEIRAS) to collect real-time signals of reaction intermediates during the OER process. As shown in Figure 5D, with increased potential, the *in situ* ATR-SEIRAS spectra of ac-FeCoNiMo reveal an absorption peak at 1,230 cm^{-1}, which is attributed to the stretching vibrations of $*O_2^{2-}$, and no *OOH intermediate was detected at 1,018 cm^{-1}, further confirming that only the LOM pathway is active on the surface. Therefore, ac-FeCoNiMo follows the LOM mechanism (steps shown in Figure 5A) for the OER process, originating from the weakened metal-oxygen bonds by incorporating the high valence state of Mo element to enlarge the M-O-M units and form the abundant rich bounds.

CONCLUSIONS

In summary, we designed a high OER electrocatalyst ac-FeCoNiMo by creating a boundary-rich crystalline/amorphous heterostructure, modulated electronic structure of Fe/Co species and defects via introducing

high valence metal Mo into a multicomponent transition metal matrix. Furthermore, ac-FeCoNiMo exhibited an increased specific surface area and optimized pore size distribution. As a result, ac-FeCoNiMo achieved low overpotentials of 222 mV and 253 mV at current densities of 20 mA cm^{-2} and 100 mA cm^{-2}, respectively, while displaying excellent stability, which was superior to the benchmark RuO_2. The mechanism investigation indicates ac-FeCoNiMo follows LOM mechanism during the OER process, which can be ascribed to the induced weakened metal-oxygen bonds with the enlarged M-O-M units and the formation of the abundant rich boundaries. This work opens a new venue for developing highly efficient multi-element electrocatalysts and potential high-entropy materials for OER.

DECLARATIONS

Acknowledgments

All authors appreciate the support from the "Joint International Laboratory on Environmental and Energy Frontier Materials" and "Innovation Research Team of High-Level Local Universities in Shanghai".

Authors' contributions

Contributed equally to this work: Li, L.; Wu, J.
Supervised the research: Liu, Hao.; Zhao, Y.; Zhang, J.
Designed the research: Li, L.; Wu, J.; Zhao, Y.
Conducted the various *in situ* measurements: Sun, L.
Participated in catalyst synthesis and characterization: Cao, X.; Pan, F.; Gao, L.
Analyzed the data: Zhao, Y.; Gao, H.
Co-wrote the paper: Wu, J.; Li, L.
Participated in the discussion: Li, D.; Zhang, Y.; Li, Q.
All authors revised the manuscript and have given approval to the final version of the manuscript.

Availability of data and materials

The data supporting the findings of this study are available within this Article and its Supplementary Materials. Further data are available from the corresponding authors upon request.

Financial support and sponsorship

This work was supported by the National Natural Science Foundation of China (22209103). Zhao, Y. and Li, Q. thank the UTS-HUST Key Technology Partner Seed Fund for their support. Zhang, Y. also thanks the S&T Program of Hebei for their support. Zhang, J. acknowledges support from the Australian Research Council (DE240100868). Liu, H. thanks CSIRO for support through the "International Hydrogen Research Collaboration Program-Research Fellowship".

Conflicts of interest

Liu, H. is listed as an Associate Editor of the journal *Energy Materials*. However, Hao Liu was not involved in any aspect of the editorial process, including reviewer selection, manuscript handling, or decision-making. The other authors declare that there are no conflicts of interest.

Ethical approval and consent to participate

Not applicable.

Consent for publication

Not applicable.

REFERENCES

1. Edgington, J.; Vispute, S.; Li, R.; Deberghes, A.; Seitz, L. C. Quantification of electrochemically accessible iridium oxide surface area with mercury underpotential deposition. *Sci. Adv.* **2024**, *10*, eadp8911. DOI PubMed PMC
2. Cao, X.; Huo, J.; Li, L.; et al. Recent advances in engineered Ru-based electrocatalysts for the hydrogen/oxygen conversion reactions. *Adv. Energy. Mater.* **2022**, *12*, 2202119. DOI
3. Guo, J.; Huo, J.; Liu, Y.; et al. Nitrogen-doped porous carbon supported nonprecious metal single-atom electrocatalysts: from synthesis to application. *Small. Methods.* **2019**, *3*, 1900159. DOI
4. Pei, Z.; Tan, H.; Gu, J.; et al. A polymeric hydrogel electrocatalyst for direct water oxidation. *Nat. Commun.* **2023**, *14*, 818. DOI PubMed PMC
5. Chen, X.; Zhang, Z.; Chen, Y.; et al. Research advances in earth-abundant-element-based electrocatalysts for oxygen evolution reaction and oxygen reduction reaction. *Energy. Mater.* **2023**, *3*, 300031. DOI
6. Zhao, Y.; Shen, Z.; Huo, J.; et al. Epoxy-rich Fe single atom sites boost oxygen reduction electrocatalysis. *Angew. Chem. Int. Ed.* **2023**, *62*, e202308349. DOI
7. Wang, P.; Lin, Y.; Xu, Q.; et al. Acid-corrosion-induced hollow-structured NiFe-layered double hydroxide electrocatalysts for efficient water oxidation. *ACS. Appl. Energy. Mater.* **2021**, *4*, 9022-31. DOI
8. Chen, X.; Liu, J.; Yuan, T.; et al. Recent advances in earth-abundant first-row transition metal (Fe, Co and Ni)-based electrocatalysts for the oxygen evolution reaction. *Energy. Mater.* **2022**, *2*, 200028. DOI
9. Zhao, J.; Guo, Y.; Zhang, Z.; et al. Out-of-plane coordination of iridium single atoms with organic molecules and cobalt-iron hydroxides to boost oxygen evolution reaction. *Nat. Nanotechnol.* **2025**, *20*, 57-66. DOI
10. He, B.; Deng, Q.; Wang, Y.; et al. Modification of surface electronic structure via Ru-doping: porous Ru-CoFeP nanocubes to boost the oxygen evolution reaction. *J. Power. Sources.* **2022**, *537*, 231506. DOI
11. Lei, Y.; Zhang, L.; Xu, W.; et al. Carbon-supported high-entropy Co-Zn-Cd-Cu-Mn sulfide nanoarrays promise high-performance overall water splitting. *Nano. Res.* **2022**, *15*, 6054-61. DOI
12. Xu, H.; Yang, J.; Ge, R.; et al. Carbon-based bifunctional electrocatalysts for oxygen reduction and oxygen evolution reactions: optimization strategies and mechanistic analysis. *J. Energy. Chem.* **2022**, *71*, 234-65. DOI
13. Luo, Y.; Wei, L.; Geng, H.; Zhang, Y.; Yang, Y.; Li, C. C. Amorphous bimetallic oxides Fe-V-O with tunable compositions toward rechargeable Zn-Ion batteries with excellent low-temperature performance. *ACS. Appl. Mater. Interfaces.* **2020**, *12*, 11753-60. DOI
14. Wang, Y.; Zhang, L.; Meng, X.; et al. Scalable processing hollow tungsten carbide spherical superstructure as an enhanced electrocatalyst for hydrogen evolution reaction over a wide pH range. *Electrochim. Acta.* **2019**, *319*, 775-82. DOI
15. Gultom, N. S.; Abdullah, H.; Hsu, C.; Kuo, D. Activating nickel iron layer double hydroxide for alkaline hydrogen evolution reaction and overall water splitting by electrodepositing nickel hydroxide. *Chem. Eng. J.* **2021**, *419*, 129608. DOI
16. Hao, H.; Li, Y.; Wu, Y.; et al. In-situ probing the rapid reconstruction of FeOOH-decorated $NiMoO_4$ nanowires with boosted oxygen evolution activity. *Mater. Today. Energy.* **2022**, *23*, 100887. DOI
17. Xiao, Y.; Chen, X.; Li, T.; et al. Mo-doped cobalt hydroxide nanosheets coupled with cobalt phosphide nanoarrays as bifunctional catalyst for efficient and high-stability overall water splitting. *Int. J. Hydrogen. Energy.* **2022**, *47*, 9915-24. DOI
18. Jin, Y.; Huang, S.; Yue, X.; Du, H.; Shen, P. K. Mo- and Fe-modified $Ni(OH)_2$/NiOOH nanosheets as highly active and stable electrocatalysts for oxygen evolution reaction. *ACS. Catal.* **2018**, *8*, 2359-63. DOI
19. Xiong, S.; Wang, L.; Chai, H.; Xu, Y.; Jiao, Y.; Chen, J. Molybdenum doped induced amorphous phase in cobalt acid nickel for supercapacitor and oxygen evolution reaction. *J. Colloid. Interface. Sci.* **2022**, *606*, 1695-706. DOI
20. Su, X.; Wang, Y.; Zhou, J.; Gu, S.; Li, J.; Zhang, S. Operando spectroscopic identification of active sites in nife prussian blue analogues as electrocatalysts: activation of oxygen atoms for oxygen evolution reaction. *J. Am. Chem. Soc.* **2018**, *140*, 11286-92. DOI
21. Shi, Z.; Yu, Z.; Guo, J.; et al. Lattice distortion of crystalline-amorphous nickel molybdenum sulfide nanosheets for high-efficiency overall water splitting: libraries of lone pairs of electrons and in situ surface reconstitution. *Nanoscale* **2022**, *14*, 1370-9. DOI
22. Chen, Z. J.; Zhang, T.; Gao, X. Y.; et al. Engineering microdomains of oxides in high-entropy alloy electrodes toward efficient oxygen evolution. *Adv. Mater.* **2021**, *33*, 2101845. DOI
23. Qiu, Y.; Jia, Q.; Yan, S.; Liu, B.; Liu, J.; Ji, X. Favorable amorphous-crystalline iron oxyhydroxide phase boundaries for boosted alkaline water oxidation. *ChemSusChem* **2020**, *13*, 4911-5. DOI
24. Sheng, H.; Qu, H.; Zeng, B.; et al. Enriched Fe doped on amorphous shell enable crystalline@amorphous core-shell nanorod highly efficient electrochemical water oxidation. *Small* **2023**, *19*, 2300876. DOI
25. Li, D.; Qin, Y.; Liu, J.; et al. Dense crystalline-amorphous interfacial sites for enhanced electrocatalytic oxygen evolution. *Adv. Funct. Mater.* **2022**, *32*, 2107056. DOI
26. Zhang, B.; Zheng, X.; Voznyy, O.; et al. Homogeneously dispersed multimetal oxygen-evolving catalysts. *Science* **2016**, *352*, 333-7. DOI
27. Zhang, Y.; Gao, F.; Wang, D.; et al. Amorphous/crystalline heterostructure transition-metal-based catalysts for high-performance water splitting. *Coord. Chem. Rev.* **2023**, *475*, 214916. DOI

28. Lyons, M. E.; Floquet, S. Mechanism of oxygen reactions at porous oxideelectrodes. Part 2-oxygen evolution at RuO_2, IrO_2 and $Ir_xRu_{1-x}O_2$ electrodes in aqueous acid and alkaline solution. *Phys. Chem. Chem. Phys.* **2011**, *13*, 5314-35. DOI PubMed
29. Fan, X.; Liu, Y.; Chen, S.; et al. Defect-enriched iron fluoride-oxide nanoporous thin films bifunctional catalyst for water splitting. *Nat. Commun.* **2018**, *9*, 1809. DOI PubMed PMC
30. Luo, M.; Zhao, Z.; Zhang, Y.; et al. PdMo bimetallene for oxygen reduction catalysis. *Nature* **2019**, *574*, 81-5. DOI
31. Li, S.; Bai, L.; Shi, H.; et al. Mo-doped CoP nanosheets as high-performance electrocatalyst for HER and OER. *Ionics* **2021**, *27*, 3109-18. DOI
32. Liu, Y.; Liu, P.; Men, Y. L.; et al. Incorporating MoO_3 patches into a Ni oxyhydroxide nanosheet boosts the electrocatalytic oxygen evolution reaction. *ACS. Appl. Mater. Interfaces.* **2021**, *13*, 26064-73. DOI
33. Yu, L.; Wu, L.; Mcelhenny, B.; et al. Ultrafast room-temperature synthesis of porous S-doped Ni/Fe (oxy)hydroxide electrodes for oxygen evolution catalysis in seawater splitting. *Energy. Environ. Sci.* **2020**, *13*, 3439-46. DOI
34. Wang, H.; Qi, J.; Yang, N.; et al. Dual-defects adjusted crystal-field splitting of $LaCo_{1-x}Ni_xO_{3-\delta}$ hollow multishelled structures for efficient oxygen evolution. *Angew. Chem. Int. Ed.* **2020**, *59*, 19691-5. DOI
35. Pan, Y.; Gao, J.; Lv, E.; et al. Integration of alloy segregation and surface Co-O hybridization in carbon-encapsulated CoNiPt alloy catalyst for superior alkaline hydrogen evolution. *Adv. Funct. Mater.* **2023**, *33*, 2303833. DOI
36. Jeghan, S. M. N.; Kim, J.; Lee, G. Hierarchically designed CoMo marigold flower-like 3D nano-heterostructure as an efficient electrocatalyst for oxygen and hydrogen evolution reactions. *Appl. Surf. Sci.* **2021**, *546*, 149072. DOI
37. Zhang, H.; Xia, B.; Wang, P.; et al. From waste to waste treatment: mesoporous magnetic $NiFe_2O_4$/ZnCuCr-layered double hydroxide composite for wastewater treatment. *J. Alloys. Compd.* **2020**, *819*, 153053. DOI
38. He, R.; Li, M.; Qiao, W.; Feng, L. Fe doped Mo/Te nanorods with improved stability for oxygen evolution reaction. *Chem. Eng. J.* **2021**, *423*, 130168. DOI
39. Huang, Y.; Wu, Y.; Zhang, Z.; Yang, L.; Zang, Q. Rapid electrodeposited of self-supporting Ni-Fe-Mo film on Ni foam as affordable electrocatalysts for oxygen evolution reaction. *Electrochim. Acta.* **2021**, *390*, 138754. DOI
40. Wei, Y.; Li, W.; Li, D.; Yi, L.; Hu, W. Amorphous-crystalline cobalt-molybdenum bimetallic phosphide heterostructured nanosheets as Janus electrocatalyst for efficient water splitting. *Int. J. Hydrogen. Energy.* **2022**, *47*, 7783-92. DOI
41. Ali, U.; Sohail, K.; Liu, Y.; Yu, X.; Xing, S. Molybdenum and phosphorous dual-doped, transition-metal-based, free-standing electrode for overall water splitting. *ChemElectroChem* **2021**, *8*, 1612-20. DOI
42. Ma, Y.; Dong, X.; Wang, Y.; Xia, Y. Decoupling hydrogen and oxygen production in acidic water electrolysis using a polytriphenylamine-based battery electrode. *Angew. Chem. Int. Ed.* **2018**, *57*, 2904-8. DOI
43. Zhang, Z.; Jia, C.; Ma, P.; et al. Distance effect of single atoms on stability of cobalt oxide catalysts for acidic oxygen evolution. *Nat. Commun.* **2024**, *15*, 1767. DOI PubMed PMC
44. Zhang, M.; Liu, Y.; Liu, B.; Chen, Z.; Xu, H.; Yan, K. Trimetallic NiCoFe-layered double hydroxides nanosheets efficient for oxygen evolution and highly selective oxidation of biomass-derived 5-hydroxymethylfurfural. *ACS. Catal.* **2020**, *10*, 5179-89. DOI
45. Ye, C.; Wang, M. Q.; Bao, S. J.; Ye, C. Micropore-boosted layered double hydroxide catalysts: EIS analysis in structure and activity for effective oxygen evolution reactions. *ACS. Appl. Mater. Interfaces.* **2019**, *11*, 30887-93. DOI PubMed
46. Sun, S.; Li, H.; Xu, Z. J. Impact of surface area in evaluation of catalyst activity. *Joule* **2018**, *2*, 1024-7. DOI
47. Wei, C.; Xu, Z. J. The Comprehensive Understanding of $^{10mA\ cm_{ox}^{-2}}$ as an evaluation parameter for electrochemical water splitting. *Small. Methods.* **2018**, *2*, 1800168. DOI
48. Yang, H.; Wang, C.; Zhang, Y.; Wang, Q. Green synthesis of NiFe LDH/Ni foam at room temperature for highly efficient electrocatalytic oxygen evolution reaction. *Sci. China. Mater.* **2019**, *62*, 681-9. DOI
49. Xie, Y.; Luo, F.; Yang, Z. Acidic oxygen evolution reaction via lattice oxygen oxidation mechanism: progress and challenges. *Energy. Mater.* **2025**, *5*, 500026. DOI